

Autonomous Distributed LQR/APF Control Algorithm for Multiple Small Spacecraft during Simultaneous Close Proximity Operations

Shawn B. McCamish
 PhD Candidate, Major, USAF
 U. S. Naval Postgraduate School (NPS), Monterey, California
 Email: sbmccami@nps.edu

Marcello Romano
 Assistant Professor, MAE Department, NPS
 Email: mromano@nps.edu

Xiaoping Yun
 Professor, ECE Department, NPS
 Email: xyun@nps.edu

ABSTRACT

An autonomous distributed LQR/APF control algorithm for multiple small spacecraft during simultaneous close proximity operations has been developed. This research contributes to the control of multiple small spacecraft for emerging operation, which may include inspection, assembly, or servicing. A control algorithm is proposed which combines the control effort efficiency of the Linear Quadratic Regulator (LQR) and the robust collision avoidance capability of the Artificial Potential Function (APF) methods. The LQR control effort serves as the attractive force toward goal positions, while APF-based repulsive functions provide collision avoidance for both fixed and moving obstacles. Refinement of both the APF and LQR control algorithms to small spacecraft applications offered insight and enhancement of the resulting control algorithm. Comprehensive performance evaluation of the multiple small spacecraft LQR/APF control algorithm is conducted for simultaneous close proximity maneuvers, such as convergence, rally, rendezvous, and docking maneuvers. These simulations show the developed LQR/APF control algorithm to be both robust and efficient based on the primary metrics of maneuver duration and required Δv . Promising simulation results are presented for simultaneous multiple small spacecraft gathering, rendezvous, and docking maneuvers.

INTRODUCTION

Simultaneous control of multiple small spacecraft maneuvers is required for several planned space missions in the near future.¹⁻² Large spacecraft formation tracking and station keeping has received a great deal of study, but research in the area of multiple small spacecraft close proximity operations is limited.³⁻⁴ There are numerous mission scenarios that involve the divergence or convergence of multiple spacecraft in close proximity.⁵⁻⁹ Currently these maneuvers are pre-determined and performed with centralized control. Typical close proximity path planning and tracking algorithms are computationally expensive, and may require manual back-up.

Therefore, a relatively simple control algorithm is desired which allows for multiple small spacecraft close proximity operations. Research and experience with terrestrial based robots have matured the application of artificial potential function (APF) based robotic navigation and control algorithms. The simplicity of

the APF based control algorithms is a good match for small spacecraft application with limited proximity sensors and processing capability. During control algorithm development, global knowledge is assumed not to be available to each agent.³ Also, a centralized controller is assumed not to exist, such that each agent must perform their portion of the operation with local information and limited communications. Previously proposed spacecraft APF based controllers have been very task specific and not robust in the full range of possible close proximity operations.¹⁰⁻¹¹ Also, studies of their efficiency have primarily been focused on maintaining spacecraft trajectories and formations.¹² The consideration of efficiency while maintaining collision avoidance in close proximity operations has been particularly limited, and usually requires dramatic increases in computation or centralization. Our research expands on the development of a control algorithm which combines the efficiency of Linear Quadratic Regulator (LQR) with APF-based collision avoidance concepts.¹³ The APF-based collision

avoidance relies on relative positions and velocities, as opposed to only position, for controlling spacecraft. The developed LQR/APF multiple spacecraft close proximity control algorithm offers robust close proximity performance and establishes a reliable baseline for control effort efficiency while maintaining collision free maneuvers. The merged LQR/APF control algorithm utilizes simple goal commands and obstacle sensory data. This control approach is refined, from the previous development in Ref. 13, and applied to nonlinear multiple spacecraft dynamics and kinematics models.

Critical evaluation of multiple spacecraft control algorithms requires high fidelity six degree of freedom (6-DOF) spacecraft models. Most proposed spacecraft control algorithms have not been fully assessed with realistic spacecraft dynamics, kinematics, and constraints. The spacecraft's physical characteristics and actuator constraints must be included in order to determine if a spacecraft control algorithm is practical and valid. The developed LQR/APF multiple spacecraft close proximity control algorithm allows for convenient inclusion of known or estimated sensor uncertainties and actuator response into the control parameters. An uncoupled attitude control loop allows for orientation changes during all maneuvers.

This paper outlines the development, refinement, and evaluation of the autonomous distributed LQR/APF control algorithm for multiple small spacecraft. The relative dynamic equations of motion between multiple spacecraft in close proximity and a high fidelity 6-DOF small spacecraft model are discussed. Our refined LQR/APF proximity spacecraft control algorithm, based on LQR and APF concepts is developed and evaluated. The simultaneous spacecraft motion scheme is extended to include collision and obstacle avoidance while conducting close proximity maneuvers with six Chase spacecraft. These six simultaneously maneuvering Chase Spacecraft are evaluated during convergence, rally, rendezvous, and docking operations. The LQR/APF control algorithm's promising results, based on short maneuver durations with limited control effort, paves the way for potential application to a wide range of multiple small spacecraft close proximity operations.

OVERVIEW OF RELATIVE SPACECRAFT MODEL

The first computational step in developing a control algorithm is to establish the system model. For this research, the fundamental system is a 6-DOF small spacecraft orbiting the Earth. The control algorithm employs linearized relative motion equations, but all

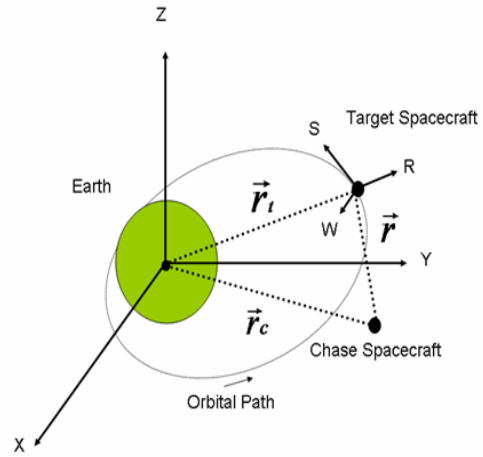


Figure 1: Relative Reference Frame

numerical simulations are driven by the nonlinear spacecraft model including main perturbations.

Linear model of Multiple Spacecraft Relative Motion

As usual, the Earth Centered Inertial (ECI) coordinate system (X,Y,Z) and the Local Vertical-Local Horizontal coordinate system (R,S,W), as depicted in Fig. 1, are used to describe the motion dynamics.¹⁴ In order to establish the equations of motion between spacecraft we will consider one of the spacecraft as primary spacecraft (Target) and all others as secondary spacecraft (Chasers). The Hill-Clohesy-Wiltshire linearized equations of relative motion¹⁵

$$\begin{aligned} \ddot{x} - 2(\omega \cdot \dot{y}) - 3(\omega^2 \cdot x) &= a_x & (a) \\ \ddot{y} + 2(\omega \cdot \dot{x}) &= a_y & (b) \\ \ddot{z} + (\omega^2 \cdot z) &= a_z & (c) \end{aligned} \quad (1)$$

where x , y , and z are relative position states, ω is the Target spacecraft's orbital angular velocity, and $a_{x,y,z}$ are the axial accelerations due to control effort.. These equations can be written in general state space form as:

$$\begin{bmatrix} \dot{x} \\ \dot{y} \\ \dot{z} \\ \ddot{x} \\ \ddot{y} \\ \ddot{z} \end{bmatrix} = \begin{bmatrix} 0 & 0 & 0 & 1 & 0 & 0 \\ 0 & 0 & 0 & 0 & 1 & 0 \\ 0 & 0 & 0 & 0 & 0 & 1 \\ 3\omega^2 & 0 & 0 & 0 & 2\omega & 0 \\ 0 & 0 & 0 & -2\omega & 0 & 0 \\ 0 & 0 & -\omega^2 & 0 & 0 & 0 \end{bmatrix} \begin{bmatrix} x \\ y \\ z \\ \dot{x} \\ \dot{y} \\ \dot{z} \end{bmatrix} + \begin{bmatrix} 0 & 0 & 0 \\ 0 & 0 & 0 \\ 0 & 0 & 0 \\ 1 & 0 & 0 \\ 0 & 1 & 0 \\ 0 & 0 & 1 \end{bmatrix} \begin{bmatrix} a_x \\ a_y \\ a_z \end{bmatrix} \quad (2)$$

The linear dynamics are used for control algorithm design; while the full spacecraft model, as described in the following section, is exploited during numerical simulations.¹⁴

High Fidelity Spacecraft Model

Performance evaluation on a validated model is a critical part of control algorithm development. An effective test scenario is one which dependably simulates the environment in which the control algorithm is expected to operate. The application of the control algorithm for use on multiple small spacecraft in proximity operations drives the requirements that it be tested with computer-generated orbital dynamics and kinematics. For this research a high fidelity 6-DOF spacecraft dynamics model is used. Given the initial values of the relative position and velocity of the spacecraft, the orbit is propagated by numerical integrations. In particular, a fourth-order Runge-Kutta method was used with $\Delta t = 1.0$ s time increment. This conservative bandwidth was selected to allow for slow actuation cycles and sensor update rates. The spacecraft model was developed in MATLAB¹⁶ and validated via STK¹⁷. A full overview of the model and simulation developed for the multiple spacecraft close proximity control algorithm is discussed in Ref. 18.

The physical characteristics of each small spacecraft in the group are assumed to be the similar. The Target spacecraft orbital altitude is assigned a predetermined, or randomly distributed, range of 300-2,000 km. The number of Chase spacecraft is assigned, or randomly selected, from 1-6. Each Chase spacecraft is assigned a predetermined, or randomly distributed, initial position from the Target spacecraft's initial position. This initial range between the Target and Chaser spacecraft is within 1,000 m in RSW coordinates. Initial velocities of the Chase spacecraft are assumed to be the same as the Target spacecraft. This neutral initial velocity allows for practical controller performance evaluation. The simulation condition ranges are summarized in Table 1.

The small cubic spacecraft considered in this research are 1.0 m in width and 100 kg in mass, following the subsystem sizing guidelines from Ref. 19. The center of mass of the spacecraft is assumed to be located at the geometric center. Position and ranging sensors are

Table 1: Close Proximity Maneuver Parameters

Target Spacecraft	Min Altitude	300 km
	Max Altitude	2,000 km
Chase Spacecraft	Number	1-6
Chase Spacecraft Initial Position	R-axis	1.0 -1,000 m
	S-axis	1.0 -1,000 m
	W-axis	1.0 -1,000 m
Chase Spacecraft Initial Velocity	R-axis	0.0 m/s
	S-axis	0.0 m/s
	W-axis	0.0 m/s

assumed to provide ideal information. The commanded translational motion is conducted via thrusters with a maximum thrust of 1.0 N along each of the three primary axes. Based on standard measures of propulsion system performance, the estimated lifetime Δv for each spacecraft is between 20-120 m/s. The total thruster Δv for each maneuver serves as a metric for evaluating control algorithm performance. The attitude control of the spacecraft is uncoupled from the translational thrusters. Attitude control utilizes nonlinear quaternion feedback. The quaternion feedback control commands three orthogonal reaction wheels each with magnetotorquers for momentum damping; refer to Ref. 20 and Ref. 21 for detailed discussions. The general sizing and performance ranges of the modeled actuators are listed in Table 2.

Table 2: Small Spacecraft Characteristics

Physical Properties	Length/Width	1.0 m
	Height	1.0 m
	Mass	100 kg
	Moment of Inertia X	16.67 kg m ²
	Moment of Inertia Y	16.67 kg m ²
	Moment of Inertia Z	16.67 kg m ²
Actuators	Number of Thrusters	1-6
	Initial Propellant	3-6%
	Specific Impulse	100-200 s
	Max Thrust per axis	1.0 N
	Reaction Wheels (RW)	3
	RW Max Torque	0.055 N m
	RW Max Ang. Mom.	4-12 N m s
	Initial RW Ang. Rate	0 RPM
	RW spin axis Inertia	0.1426 kg m ²
	Magnetotorquers	3
	Max dipole moment	100 A m ²
	Docking Tolerances	Max Axial
Max Lateral		+/- 2.0 mm
Max Angular		+/- 0.1 deg

The inclusion of attitude control allows rotation of the Chase spacecraft, which required modification to the collision avoidance. The cubic shape of the small spacecraft and the freedom of rotation in the vicinity of obstacles required the obstacle avoidance logic to be modified for robustness. The Chase spacecraft's is commanded to point toward the goal location for most maneuvers and along the port axis for docking.

The orbital perturbations included in the spacecraft dynamics model are non-symmetrical earth (J2-J4), atmospheric drag, third body (Sun and Moon) effects, and solar radiation pressure; refer to Ref. 14 and Ref. 17 for full development. This research treats the spacecraft as a *black body* and uses the Earth Gravity Model (EGM-96) coefficients and World Geodetic

System (WGS-84) reference shape for calculations.¹⁴ The significance of these perturbation forces vary due to spacecraft size, position and altitude. Additionally, the mass variation due to commanded thruster firings is incorporated into the spacecraft model.

CLOSE PROXIMITY MULTIPLE SPACECRAFT LQR CONTROL ALGORITHM

The first step in our control algorithm research is to develop a close proximity multiple spacecraft LQR controller. The LQR algorithm serves as the principal convergence force during close proximity operations. The multiple spacecraft LQR algorithm uses the linearized state dynamics from Eq. (2). The iterative LQR allows for efficient control effort based on optimal cost for dynamic system states. Each LQR solution is optimal for the current cost function. The cost function is based on variable gain matrixes, which allow for steady convergence to the desired goal state.

Overview of LQR Control Algorithm

The LQR quadratic cost function is of the general form

$$J = (1/2) \cdot \int_0^T (x^T \cdot Q \cdot x + u^T \cdot R \cdot u) dt \quad (3)$$

where Q is the state gain matrix and R is the control effort gain matrix. This optimal feedback control is given by the well known expression

$$u = -R^{-1} \cdot (B^T \cdot S) \cdot x = -K_{LQR} \cdot x \quad (4)$$

where K_{LQR} is the optimal state feedback and S is the solution of the algebraic Riccati equation. This LQR determined control effort, u , is the desired acceleration due to the actuators, \bar{a}_{LQR} . The weighting matrixes can be selected in order to trade-off state convergence and the control effort efficiency. For relative spacecraft position and velocity states with control effort along each axis, the LQR gain matrixes are of the form

$$Q = \begin{bmatrix} \frac{\alpha_{Q_1}}{(x_{\max})^2} & 0 & 0 & 0 & 0 & 0 \\ 0 & \frac{\alpha_{Q_2}}{(y_{\max})^2} & 0 & 0 & 0 & 0 \\ 0 & 0 & \frac{\alpha_{Q_3}}{(z_{\max})^2} & 0 & 0 & 0 \\ 0 & 0 & 0 & \frac{\alpha_{Q_4}}{(\dot{x}_{\max})^2} & 0 & 0 \\ 0 & 0 & 0 & 0 & \frac{\alpha_{Q_5}}{(\dot{y}_{\max})^2} & 0 \\ 0 & 0 & 0 & 0 & 0 & \frac{\alpha_{Q_6}}{(\dot{z}_{\max})^2} \end{bmatrix} \quad (5)$$

$$R = \begin{bmatrix} \frac{\beta_{R_1}}{(u_{x\max})^2} & 0 & 0 \\ 0 & \frac{\beta_{R_2}}{(u_{y\max})^2} & 0 \\ 0 & 0 & \frac{\beta_{R_3}}{(u_{z\max})^2} \end{bmatrix} \quad (6)$$

As an initial guess, the gain matrixes are typically selected as diagonal matrices with elements' values normalized by the maximum allowable values of states, x_{\max} , y_{\max} , and z_{\max} , and control efforts, $u_{x\max}$, $u_{y\max}$, and $u_{z\max}$. The selection of diagonal weighting numerator gains α_Q and β_R , for Q and R respectively, can be fine tuned based on simulation results.

Close Proximity Spacecraft LQR Gain Selections

For our research, the LQR gain matrixes for spacecraft close proximity maneuvers are selected for efficient control effort and relatively short maneuver duration. The LQR gains for weighting matrixes were refined while evaluating control response and comparing with refined APF control responses. As spacecraft converge, the cost slope for fixed gain control tends to flatten due to the small state values being considered. This leveling of the cost in the vicinity of the goal can be avoided by using variable gains. Proper gain selections permit steady cost convergence even in the immediate vicinity of the goal. This controller characteristic is essential for sub-meter spacecraft docking precision.

The LQR state gain matrix scales the Chase spacecraft's relative position and velocity as it approaches the goal. The relative position error along each axis is equally weighted by Euclidean (2-norm) of the Chase spacecraft three-dimensional position vector from the goal, r_g , by selecting $x_{\max} = y_{\max} = z_{\max} = r_g$ in Eq. (5). Selecting the position gain denominator to be the current distance to the goal allows relative position to become more important as the spacecraft approaches the goal. The relative velocity error along each axis is also equally weighted, by selecting $\dot{x}_{\max} = \dot{y}_{\max} = \dot{z}_{\max} = (r_{init}/r_m) \cdot v_m$ in Eq. (5). This velocity term is determined by scaling the maximum allowed relative Chase spacecraft velocity, v_m by the ratio of the Chase spacecraft's initial range, r_{init} , and the Chase spacecraft's maximum range, r_m . The maximum relative Chase spacecraft velocity should be

selected based on available spacecraft actuation and desired maneuver duration. Conservative selection will limit the transients due to the initially neutral relative velocity and the convergence rate for safe operations. The numerator terms for the diagonal gains of Eq. (5) are chosen to be $\alpha_{Q_1} = \alpha_{Q_2} = \alpha_{Q_3} = \alpha_{Q_4} = \alpha_{Q_5} = \alpha_{Q_6} = r_g$.

The actuator control effort is the acceleration imparted due to translational thrusters. The denominator terms for the diagonal control effort gains in Eq. (6) are selected to be $u_{x\max} = u_{y\max} = u_{z\max} = a_m$. The control effort gains are also scaled as the spacecraft relative position changes by selecting $\beta_{R_1} = \beta_{R_2} = \beta_{R_3} = r_g$ in Eq. (6). A minimum scaling factor for the numerator gains can be selected so that, as the range to goal approaches zero, numerical problems and chattering are avoided. For instance as the r approaches zero the value of r is limited to some minimum value, such as $\beta_R \geq 0.05$.

CLOSE PROXIMITY MULTIPLE SPACECRAFT APF CONTROL ALGORITHM

Next, we developed a multiple spacecraft APF control algorithm with collision avoidance. Our research explores the use of potential functions in relation to velocity error, as opposed to only position errors, for controlling spacecraft. An advantage of the space environment is that it is relatively obstacle free and obstacles are of limited size. In addition, obstacles crossing the orbital path will usually be at high enough relative velocity that collision avoidance maneuvers are not necessary, or possible, for a spacecraft with limited actuation and local sensor information. The APF control algorithm's collision avoidance capability is essential during simultaneous multiple spacecraft close proximity maneuvers.

Overview of APF Control Algorithm

APF theory has been used extensively in robot navigation and control.²²⁻²⁸ APF control algorithms are effective in simple obstacle environments and safer than most path planning algorithms in highly dynamic environments. APF guidance was considered for orbital vehicles by McInnes in 1993.²⁹ It has been expanded to consider distributed control,³⁰ autonomous rendezvous with fixed obstacle avoidance,³¹ autonomous control of on-orbit assembly,³² and fuel efficiency constraints for cluster formation maintenance.³³ Recent application of APF for swarm control of micro-utility spacecraft also shows promise.¹⁰⁻¹¹

In general, the APF of each spacecraft is determined by the arithmetic superposition of the goal and all obstacle potential functions in its working area.²⁴ The overall potential field will serve as the performance surface for the control algorithm, of the form

$$V = V_g + V_o \quad (7)$$

where V_g is the attractive potential of the goal point and V_o is the repulsive potential of obstacles. Selection of the potential functions is critical in ensuring smooth potential fields that are stable and provide the desired performance. One strategy is to select quadratic potential functions, based on the desirable characteristics of Lyapunov functions.³⁴ The desired velocity can converge along the negative potential gradient as the potential decreases to zero. The attractive and repulsive potential are related to desired control forces.

Spacecraft APF Control Algorithm Development

Although the goal potential attraction is later replaced by the LQR, it was used for comparison purposes in our simulations. The APF goal and obstacle potentials were refined for close proximity relative spacecraft control. The goal, or attractive, potential was chosen as

$$V_g = (\lambda_g / 2) \cdot r_g^2 \quad (8)$$

where λ_g is the non-negative goal potential shaping parameter. For this research, $\lambda_g = 1/r_g$ was selected. This allows the usual quadratic position based potential to be replaced with the non-negative range to the goal. The resulting cone shaped potential allows for precision to be maintained in the vicinity of the goal. A shaping parameter is used to relate the magnitude of the potential function to desired velocity. The desired non-negative velocity shaping function was determined to be

$$k_g = (r_{init} / r_m) \cdot v_m \cdot \left(1 - e^{-(b_g \cdot v_g)} \right) \quad (9)$$

where b_g is the goal velocity decay shaping parameter. The selection of k_g determines the convergence of the control algorithm, and is especially important in the spacecraft environment. Large values cause the algorithm to converge quickly toward the area of the goal position but oscillate around the actual goal position. Small values ensure slow steady convergence toward the goal position in a damped manner. This is the more desirable of the possible behaviors for

multiple spacecraft convergence. The parameter, b_g , is used to shape the exponential decay of the Chase spacecraft's velocity as it approaches the goal position:

$$b_g = (1/d_g) \cdot (r_m / r_{init}) \quad (10)$$

where d_g is a positive constant used to shape the velocity decay. Based on an assumption of zero starting relative velocity, the initial velocity transient is often large and causes the control actuator to saturate, as discussed in Ref. 13. In order to avoid this saturation a velocity ramping function, k_R , can be incorporated, such that

$$k_R = (d_R / r_{init}) (1 - e^{-t}) \quad (11)$$

with the velocity ramping constant, d_R , and a time parameter, t . This ramping term only influences the initial velocity transient by allowing a gradual velocity start-up of the APF control algorithm, which allows for a comparable performance with the LQR algorithm. The resulting Chase spacecraft's desired velocity based on the attraction potential toward the goal position is

$$\vec{v}_g = -k_R \cdot k_g \cdot (\nabla V / |\nabla V|) \quad (12)$$

This desired velocity is along the negative of the gradient. The actual relative velocity is subtracted from the desired velocity to determine the Δv required by the control effort, and the related spacecraft acceleration is

$$\vec{a}_g = (\vec{v}_g - \vec{v}) / \Delta t \quad (13)$$

The goal potential allows for convergence to the goal position; however an obstacle potential is required to avoid collision with other spacecraft and sensed objects. The repulsion potential curve is a smooth function that increases from the boundary of the region of influence to the surface of the obstacle. The obstacle potential is selected to be a Gaussian function of the form

$$V_o = \lambda_o \cdot \left(e^{-r_o^2 / (2 \cdot \sigma^2)} - e^{-D_o^2 / (2 \cdot \sigma^2)} \right) \quad (14)$$

where λ_o is the non-negative obstacle potential shaping parameter, r_o is the range of the Chase spacecraft from an obstacle, D_o is the obstacle's region of influence, and σ is the standard deviation for obstacle region of influence. Both λ_o and σ are selected to ensure that the

obstacle's region of influence is larger or equal to the actual dimensions of the object to be avoided. The obstacle shaping parameter used in this research is

$$\lambda_o = (r_{init} / 2) \cdot \left(e^{-L_o^2 / (2 \cdot \sigma^2)} - e^{-D_o^2 / (2 \cdot \sigma^2)} \right)^{-1} \quad (15)$$

where L_o is the obstacle's exterior surface. This selection of λ_o ensures that the value of V_o equals the initial value of V_g at the surface of the obstacle. The region of influence, D_o , is determined by

$$D_o = d_o \cdot \left(L_o + |\vec{v}|^2 / (4 \cdot a_m) \right) \quad (16)$$

with a positive stopping distance constant, d_o . The first term in Eq. (16) is a safety margin based on the size of the obstacle and the second term is the minimum stopping distance of the spacecraft. The minimum stopping distance is the only achievable by using the maximum control actuation to stop.

The standard deviation, σ , is selected so that the obstacle surface is within one standard deviation as the spacecraft relative velocity approaches zero, such that

$$\sigma = D_o / 3 \quad (17)$$

This relationship, modified from Ref. 13, allows a reasonable safety region around obstacles and a smooth Gaussian repulsive potential function. Numerous other functions could be selected for the obstacle avoidance potential, such as spherical power-law and super quadratic functions.³² However, these functions would require further a priori knowledge of obstacles which are not assumed in our work.

The obstacle potential is used to modify the desired relative velocity of the chase spacecraft. The desired velocity due to an obstacle is

$$\vec{v}_o = k_o \cdot \left(\vec{r}_o / r_o \right) \quad (18)$$

where the velocity shaping function is

$$k_o = k_g \cdot V_o / (r_{init} / 2) \quad (19)$$

The attractive velocity vector due to the goal is toward the goal position and the repulsive velocity vector due to obstacles is away from each obstacle. The total control force is determined by vector addition of the

potential derived velocities minus the current actual velocity vector of the Chase spacecraft, as

$$\bar{a} = \left(\bar{v}_g + \left(\sum_{obs=0}^n \bar{v}_o \right) - \bar{v} \right) / \Delta t \quad (20)$$

with the number of obstacles, n , being limited for practical spatial applications. Obstacles may be either other spacecraft (additional Chase spacecraft converging toward a goal within the same region) or stationary obstacles in fixed positions relative to the goal location (representing for instance solar panels or thruster plume exclusion zones).

Selection of the repulsion shaping parameter must be related to the attraction shaping function in order to achieve desired critically damped performance. Proper selection allows for safety in selecting goal positions and efficiency when avoiding obstacles. For instance if the region of influence of the obstacle is too small and the slope of the repulsive potential shaping parameter is too steep then a thrust limited actuator may not be able to avoid collision with the obstacle. On the other hand, if the obstacle region is too large then the Chase spacecraft may be less efficient in both control effort and maneuver duration as it avoids obstacles.

An obstacle's repulsive region of influence may cause a local minimum or saddle point to occur in the area between the obstacle outer region of influence and the surface of the obstacle. The location of this local minimum depends on the obstacles location with respect to the goal position. This local minimum can cause difficulty if the overall potential function is the only driving function for determining control effort. However, the attractive and repulsive velocity shaping functions, k_g and k_o respectively, allow for velocity damping around regions of concern. This ensures that the chase spacecraft slows as it approaches the goal position and avoids obstacles. Balancing these parameters allows the goal position to be placed in the center of a spacecraft and the control algorithm to converge to the surface of the Target spacecraft. This is vital capability for docking maneuvers.

As numerous spacecraft and obstacles occupy the Chase spacecraft's region, three simple logical conditions help regulate Chase spacecraft collision avoidance motion. First, Chase spacecraft are only influenced by obstacles within the region of influence. Second, only obstacles which are at equal distance, or closer, to the goal position are allowed to influence the Chase spacecraft. For instance, the spacecraft is looking toward the goal like an automobile on the road which is only concerned with what is ahead of it and on

its sides. In most cases, other spacecraft are simply treated the same as obstacles. The third logical condition is that obstacles which are further away than the Chase's goal location are not allowed to influence the Chase spacecraft. This ensures that other spacecraft simultaneously docking on the far sides of a Target spacecraft do not limit convergence. These logical conditions limit the collision avoidance considerations needed in obstacle dense environments and are refined those presented in Ref. 13. Even with this logic, it is still practical to employ a docking safety parameter, k_s , which modifies the desired repulsive velocity between maneuvering spacecraft as they approach the goal. This safety parameter allows for collision avoidance while achieving precision convergence to the goal. This safety function between converging spacecraft multiplies \bar{v}_o and results in a modification to Eq. (18), as follows:

$$\bar{v}_o = k_s \cdot k_o \cdot (\bar{r}_o / r_o) \quad (21)$$

where k_s is usually equal to one. If $k_s=1$, then \bar{v}_o is not being influenced by the goal location. If multiple spacecraft rendezvous to the exact same goal position, this will result in a staggered convergence. The first Chase spacecraft to arrive converges to the goal position. The next Chase spacecraft has the additive repulsion of the first spacecraft and converges to a radial position further away. Any additional spacecraft will converge to a range slightly further away. This staggered cluster may be a desirable result for spacecraft rallying to an unknown formation, where additional command maneuvering may need to occur.

However, for multiple spacecraft docking maneuvers, the staggered cluster effect of the additive repulsion is not desired. In this case, the goal location is an actual Target spacecraft. To allow the later arriving spacecraft to converge toward docking while avoiding collision the safety function, k_s , is selected to be a decaying exponential of the attractive potential based on the goal position, such as

$$k_s = 1 - e^{-(v_g - L_o/2)} \quad (22)$$

This results in the repulsion due to other spacecraft decaying toward zero as the Chase spacecraft reaches the outer bound of the Target spacecraft. In this manner, multiple spacecraft are allowed to converge relatively tightly around the Target spacecraft. Limitations in the Target spacecraft's outer boundary surface area and local minima due to saddle points may cause some delays for spacecraft which arrive late.

This is only an issue for the second wave of arriving spacecraft as the first spacecraft settle into position. It is envisioned that each spacecraft would be commanded to a specific docking port; therefore clustered convergence is not a typical operational issue.

LQR/APF MULTIPLE SPACECRAFT CLOSE PROXIMITY CONTROLLER

The LQR/APF multiple spacecraft close proximity control algorithm proposed combines desirable characteristics of the LQR and APF. It uses the LQR response as the attractive force and APF-based repulsion for collision avoidance. The advantage of LQR consists in the incorporation of relative dynamics in the control algorithm. Using the simplified linear dynamics, the LQR generally improves the performance of the control algorithm with little additional computation. Meanwhile, the repulsive APF provides collision avoidance capability that LQR can not offer in a dynamic environment.

For the multiple spacecraft rendezvous problem, a critically damped relative position response with limited control effort is desired. As with all spacecraft maneuvers, control efficiency during multiple spacecraft close proximity operations must be considered. However, the close proximity maneuver is assumed to be operationally significant and must be performed in a finite duration. For this research, approximate maneuver duration of one quarter orbital period was assumed. The close proximity maneuver is considered successful when the Chase spacecraft converges within a precise range of its goal position. The precision used in this research is modified to evaluate various multiple spacecraft maneuvers, with the intent that the developed LQR/APF control algorithm performs docking maneuvers.

The balancing factor between spacecraft relative position and control effort efficiency is the relative convergence rate. However, the relative spacecraft dynamics causes rendezvous challenges if the relative convergence rate is too slow or rapid. If the rate of convergence is slow the goal position is spirally orbited as the minimal control actuation is used. The slow convergence can dramatically increase the maneuver duration as the spacecraft approaches close to the goal position. On the other hand, if the rate of convergence is too rapid limited actuation will result in collision danger due to relative position overshoot and oscillation. For this research converge maneuvers were required to be of an over damped nature. This ensures safety upon arrival to goal locations which are being approached by other spacecraft.

Multiple Spacecraft LQR with APF-Based Collision Avoidance Control Algorithm Development

Merging the LQR and APF control algorithms concepts is proposed as an efficient and capable combined algorithm. The recursive LQR is used as the attractive force and the APF-based repulsive forces are determined by obstacle locations. For the APF, relative position from goal and obstacles is used to determine desired velocity. Residuals from the desired velocity are used to command thruster firings. However, the LQR control effort varies the position and velocity based on the system linearized dynamics. This more complicated relationship requires a modification to both velocity and acceleration in the region of influence of obstacles. The result is an iterative spacecraft control algorithm which is driven by optimal LQR cost convergence, with associated dynamics, and APF-based smooth collision avoidance responses.

The APF obstacle potential parameters, represented in Eq. (14), can be combined to generate a Gaussian function which is equal to one at the obstacle boundary. This function is our LQR/APF velocity shaping parameter due to obstacle position.

$$k_v = \frac{e^{-r_o^2/(2\sigma^2)} - e^{-D_o^2/(2\sigma^2)}}{e^{-L_o^2/(2\sigma^2)} - e^{-D_o^2/(2\sigma^2)}} \quad (23)$$

This gain, k_v , will be multiplied by the component of the Chase spacecraft's relative velocity toward obstacle, \vec{v}_o . This ensures the Chase spacecraft slows to zero at the boundary of the obstacle.

Next, the attractive acceleration due to the LQR/APF recursive function is shaped. There is no change to the LQR when the Chase spacecraft is outside obstacle regions of influence. However, if the Chase is within an obstacle's influence then acceleration toward the obstacle must be decreased. The LQR/APF acceleration shaping parameter is selected as

$$k_a = e^{-d_a \cdot (r_o - L_o)} \quad (24)$$

where the positive constant, d_a , is used to establish the parameter's rate of decay. The k_a parameter is multiplied by the component of the Chase spacecraft's desired LQR acceleration in the direction of the obstacle, \vec{a}_o , to ensure that the LQR/APF does not drive into an obstacle. Finally, the safety docking parameter, from Eq. (22), is modified to replace the potential function with the Chase spacecraft's range from the goal.

$$k_s = 1 - e^{-(d_a \cdot r_g)} \quad (25)$$

The safety function allows the obstacle repulsion to decay faster as the Chase spacecraft approaches the goal position. If the obstacle is the Target spacecraft then the safety function allows the Chase to approach in the vicinity of the docking port.

The overall control effort for the multiple spacecraft LQR/APF with collision avoidance is

$$\bar{a} = \bar{a}_{LQR} - \sum_{obs=0}^n \left((k_v \cdot \bar{v}_o / \Delta t) + k_s \cdot k_a \cdot \bar{a}_o \right) \quad (26)$$

The control algorithm only decreases velocity and acceleration toward obstacles. It does not actually push away from obstacles. Therefore, densely packed stationary obstacle regions may cause the control to settle into regions other than the goal. However, the relative dynamics result in a force that helps the control algorithm escape local minimums. The consequence is similar to that achieved by APF wall-following methods.²⁷ The efficiency gained by the LQR/APF derived control effort results in a significant improvement in collision avoidance, when implemented in a limited number of obstacles environment.

SIMULATION RESULTS

Comprehensive performance evaluation of the LQR/APF and APF control algorithms was conducted for close proximity convergence, rally, rendezvous, and docking maneuvers. Results are shown for these four primary operations involving the simultaneous maneuvering of six Chase spacecraft. All close proximity operations begin when the Chase spacecraft are within 1.0 km of the goal. For comparison, each of these close proximity operations are sub divided into relatively near and far maneuvers based on the Chase spacecraft's initial position. In the near maneuvers each Chase spacecraft starts approximately 100 m away from the goal, whereas the far maneuvers start approximately 1.0 km from the goal. The convergence maneuver is simply moving to a goal position in free-space. The rally maneuver is gathering of multiple spacecraft to a common goal region in free space. Rendezvous maneuvers require the convergence of multiple spacecraft to a Target spacecraft. Docking maneuvers require precise convergence to the outer boundary of a Target spacecraft while avoiding collision.

In our simulations, the thrust along each spacecraft axis is limited to a maximum acceleration of

$a_m = (F_t / m_s) = 0.01 \text{ m} \cdot \text{s}^{-2}$, which is based on a thrust force of $F_t = 1.0 \text{ N}$ and a spacecraft mass of $m_s = 100 \text{ kg}$. The maximum relative Chase spacecraft velocity was conservatively selected to be $v_m = 1.0 \text{ m} \cdot \text{s}^{-1}$. This is rapid enough to allow for timely convergence, while being manageable with limited spacecraft actuation.

Performance evaluation requires that each maneuver is successfully accomplished without collision. The time duration and control efficiency are primary metrics for evaluating the performance of a control algorithm. These correspond to the time duration of the maneuver, t_d , is in s, and the required Δv is in m/s. These two metrics are roughly inversely related to each other. However, since these metrics are a result of the minimization of a cost or potential function with numerous constraints the relationship is not actually that simple. In this research, the maneuver duration for the close proximity operations is desired to be around 30 minutes. The control effort was desired to be both efficient and reasonable with limited actuation. Heavily saturated control effort in the collision avoidance environment is a safety concern. Control effort that heavily saturated the realistic and limited actuators is denoted with an asterisk (*).

Convergence Maneuver

The convergence maneuver is the baseline maneuver, without collision avoidance, used for determining control algorithm performance. In this maneuver, the Chase spacecraft maneuvers from its initial location to within 1.0 mm of goal position. The convergence maneuver was used to tune algorithms gains for similar performance based on maneuver duration and control effort efficiency. This range is much less than typically required for general close proximity control and serves to establish legitimacy for application of the control algorithm. The control algorithm results are listed for six independent relative near and six independent relatively far initial positions, in m, with respect to the Target's RSW coordinate system. The six near convergence maneuver performance results are listed in Table 3. The six far convergence maneuver performance results are listed in Table 4. The influence of other spacecraft and obstacles were not considered in these results.

Both the recursive LQR/APF and APF control algorithms were successful in converging to within 1.0 mm of a goal position. For both controllers, the closer maneuvers took less time to complete. The LQR/APF was more efficient with shorter duration for all initial positions shown in Table 3. The duration of some of

Table 3: Six Spacecraft Near Convergence Maneuver

Near Convergence	LQR/APF	APF
Near Convergence RSW [0, 70, 0]	$\Delta v = 0.1877$ $t_d = 1041$	$\Delta v = 0.1905$ $t_d = 1264$
Near Convergence RSW [50, -100, -50]	$\Delta v = 0.3105$ $t_d = 1068$	$\Delta v = 0.3123$ $t_d = 1298$
Near Convergence RSW [100, 100, 100]	$\Delta v = 0.4900$ $t_d = 1068$	$\Delta v = 0.5121$ $t_d = 1317$
Near Convergence RSW [100, 0, 0]	$\Delta v = 0.3077$ $t_d = 1056$	$\Delta v = 0.3215$ $t_d = 1284$
Near Convergence RSW [-50, 100, -100]	$\Delta v = 0.3889$ $t_d = 1082$	$\Delta v = 0.3912$ $t_d = 1295$
Near Convergence RSW [0, 0, 100]	$\Delta v = 0.2486$ $t_d = 1062$	$\Delta v = 0.2548$ $t_d = 1279$

Table 4: Six Spacecraft Far Convergence Maneuver

Far Convergence	LQR/APF	APF
Far Convergence RSW [0, 1000, 0]	$\Delta v = 2.5514$ $t_d = 1368$	$\Delta v = 2.2800$ $t_d = 1446$
Far Convergence RSW [412, -812, -412]	$\Delta v = 2.5454$ $t_d = 1371$	$\Delta v = 2.1884$ $t_d = 1453$
Far Convergence RSW [575, 575, 575]	$\Delta v = 2.7375$ $t_d = 1369$	$\Delta v = 2.9295$ $t_d = 1459$
Far Convergence RSW [1000, 0, 0]	$\Delta v = 3.2204$ $t_d = 1367$	$\Delta v = 3.4209^*$ $t_d = 1449$
Far Convergence RSW [0, 0, 1000]	$\Delta v = 2.0063$ $t_d = 1389$	$\Delta v = 2.0201$ $t_d = 1445$
Far Convergence RSW [707, 707, 0]	$\Delta v = 2.9865$ $t_d = 1361$	$\Delta v = 3.231$ $t_d = 1454$

the more distant maneuvers may be shorter due to the steep increase in actuation requested by the APF control algorithm. However, this is not considered significant, due to the average 30 minute maneuver duration. Although the model is limited to $0.01 \text{ m}\cdot\text{s}^{-2}$ the APF control algorithm may request more due to differences between the desired and actual velocity. The APF velocity dependence often results in actuator saturation in the vicinity of obstacles. The LQR/APF control algorithm requests a more gradual and smooth actuator performance. The actual Δv delivered by the actuators, not the Δv requested by the control law, is listed in the performance result tables.

Rally Maneuvers

The rally maneuver is the commanding of multiple spacecraft to a goal location, while ensuring collision avoidance. The goal location is free space and the maneuver ends as each Chase spacecraft approaches within 2.0 m of the mutual goal location. This

Table 5: Six Spacecraft Near Rally Maneuver

Near Rally	LQR/APF	APF
Near with Obstacle RSW [0, 70, 0]	$\Delta v = 0.3034$ $t_d = 1068$	$\Delta v = 0.2745$ $t_d = 1012$
Near with Obstacle RSW [50, -100, -50]	$\Delta v = 0.5363$ $t_d = 1075$	$\Delta v = 0.4400$ $t_d = 1017$
Near with Obstacle RSW [100, 100, 100]	$\Delta v = 0.7945$ $t_d = 1108$	$\Delta v = 0.7426$ $t_d = 1042$
Near with Obstacle RSW [100, 0, 0]	$\Delta v = 0.4487$ $t_d = 1050$	$\Delta v = 0.5370$ $t_d = 1073$
Near with Obstacle RSW [-50, 100, -100]	$\Delta v = 0.7016$ $t_d = 1159$	$\Delta v = 0.5875$ $t_d = 1027$
Near with Obstacle RSW [0, 0, 100]	$\Delta v = 0.4646$ $t_d = 1252$	$\Delta v = 0.4634$ $t_d = 1162$

Table 6: Six Spacecraft Far Rally Maneuver

Far Rally	LQR/APF	APF
Far with Obstacle RSW [0, 1000, 0]	$\Delta v = 4.1598$ $t_d = 1506$	$\Delta v = 3.7031^*$ $t_d = 1226$
Far with Obstacle RSW [412, -812, -412]	$\Delta v = 4.0729$ $t_d = 1507$	$\Delta v = 3.8766^*$ $t_d = 1219$
Far with Obstacle RSW [575, 575, 575]	$\Delta v = 4.3607$ $t_d = 1496$	$\Delta v = 4.7925^*$ $t_d = 1237$
Far with Obstacle RSW [1000, 0, 0]	$\Delta v = 4.8436$ $t_d = 1489$	$\Delta v = 4.8994^*$ $t_d = 1239$
Far with Obstacle RSW [0, 0, 1000]	$\Delta v = 3.346$ $t_d = 1552$	$\Delta v = 3.6122^*$ $t_d = 1227$
Far with Obstacle RSW [707, 707, 0]	$\Delta v = 2.7601$ $t_d = 1319$	$\Delta v = 3.111$ $t_d = 1168$

maneuver incorporates the collision avoidance between spacecraft and stationary obstacles. Stationary obstacles are placed at positions along the unobstructed path of the Chase spacecraft. These obstacles have an actual diameter of 2.0 m and are placed at worst case locations. The obstacles are placed directly along the Chase's spacecraft path when the Chase spacecraft is at maximum velocity. The results of six Chase spacecraft during the near rally maneuvers with collision avoidance are listed in Table 5. Similarly, the results of the far rally maneuver with collision avoidance are listed in Table 6.

The LQR/APF offers a more efficient and smoother performance, even in the presence of obstacles. Some of the maneuvers are performed faster due to the freedom of approaching only within 2.0 m of the goal location. This convergence rate favors the strict velocity control of the APF, but the APF continues to saturate the available control effort at the beginning of far maneuvers. The rally region must be reasonably

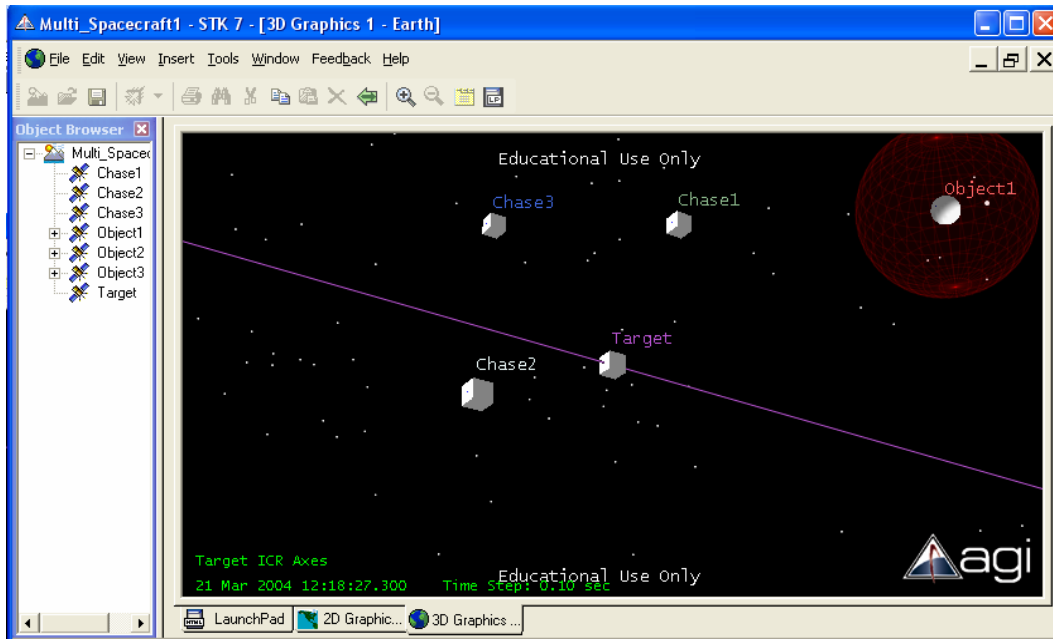


Figure 2: Simulation Rendezvous Animation Frame

adjusted as the number and size of the Chase spacecraft increase. A sample simulation animation frame is shown in Fig. 2.

Rendezvous Maneuvers

The rendezvous maneuver is intended to bring the Chase spacecraft into a predetermined range with respect to a Target spacecraft. For the general spacecraft model used in this research, the rendezvous maneuver ends as the Chase spacecraft approaches the goal within 1.0 m of the Target spacecraft's outer surface. Additionally, the LQR/APF and APF control algorithms with collision avoidance are used to avoid obstacles and other spacecraft while converging. The results for the six Chase spacecraft near rendezvous maneuver with collision avoidance are listed in Table 7, with the far results listed in Table 8. For these collision avoidance maneuvers, the goal position is the center of the Target spacecraft. This requires that the Target spacecraft's repulsion allow the Chase spacecraft to converge while avoiding impact. Stationary obstacles are once again positioned along the unobstructed path of the Chase spacecraft.

Once again, it generally takes longer for spacecraft to cover longer distance and avoiding obstacles requires more control effort and time. Notice that the APF duration for the simultaneous maneuvers increases for the latter arriving spacecraft due to repulsion of the other spacecraft. The collision avoidance algorithm logic ensures that converging spacecraft are not perturbed by latter converging spacecraft. This ensures safety in the convergence, but may cause the

Table 7: Six Spacecraft Near Rendezvous Maneuver

Near Rendezvous	LQR/APF	APF
Near with Obstacle RSW [0, 70, 0]	$\Delta v = 0.3138$ $t_d = 1066$	$\Delta v = 0.2763$ $t_d = 1011$
Near with Obstacle RSW [50, -100, -50]	$\Delta v = 0.5294$ $t_d = 1073$	$\Delta v = 0.4424$ $t_d = 1017$
Near with Obstacle RSW [100, 100, 100]	$\Delta v = 0.8096$ $t_d = 1116$	$\Delta v = 0.7362$ $t_d = 1041$
Near with Obstacle RSW [100, 0, 0]	$\Delta v = 0.4611$ $t_d = 1049$	$\Delta v = 0.5287$ $t_d = 1069$
Near with Obstacle RSW [-50, 100, -100]	$\Delta v = 0.6939$ $t_d = 1148$	$\Delta v = 0.5854$ $t_d = 1026$
Near with Obstacle RSW [0, 0, 100]	$\Delta v = 0.4604$ $t_d = 1249$	$\Delta v = 0.4551$ $t_d = 1159$

Table 8: Six Spacecraft Far Rendezvous Maneuver

Far Rendezvous	LQR/APF	APF
Far with Obstacle RSW [0, 1000, 0]	$\Delta v = 4.1568$ $t_d = 1504$	$\Delta v = 3.7170$ * $t_d = 1235$
Far with Obstacle RSW [412, -812, -412]	$\Delta v = 4.0249$ $t_d = 1499$	$\Delta v = 3.9096$ * $t_d = 1225$
Far with Obstacle RSW [575, 575, 575]	$\Delta v = 4.3766$ $t_d = 1523$	$\Delta v = 4.8191$ * $t_d = 1255$
Far with Obstacle RSW [1000, 0, 0]	$\Delta v = 4.8820$ * $t_d = 1531$	$\Delta v = 4.9273$ * $t_d = 1251$
Far with Obstacle RSW [0, 0, 1000]	$\Delta v = 3.3261$ $t_d = 1547$	$\Delta v = 3.6335$ * $t_d = 1232$
Far with Obstacle RSW [707, 707, 0]	$\Delta v = 2.8049$ $t_d = 1317$	$\Delta v = 3.1474$ $t_d = 1174$

placed at worst case locations along the Chase spacecraft's course. The generally faster convergence of the APF is as expected due to the stricter velocity maintenance of the algorithm. This is also the reason for the persistence control effort saturation.

Docking Maneuvers

The final stage and ultimate goal of rendezvous may be the docking of multiple spacecraft. The two spacecraft docking maneuver is the basis for on orbit servicing and assembly. As multiple spacecraft are required to perform docking maneuvers, several potential complications arise. First, docking of multiple spacecraft will require dedicated docking ports. Second, the docking mechanisms and the docking order need to be addressed. Third, the forces and torque tolerance of the docking mechanism and the overall spacecraft need to be considered. Also, the docking mechanisms must be arranged on each spacecraft to allow for sensor fields of view and approach zones.

For spacecraft assembly the docking order will most likely be predetermined. This is typically the case for heterogeneous spacecraft that must be assembled in a specific order.³² For homogenous spacecraft, the order of docking may not be as important, but may be limited due to docking mechanism number, position, and function. For instance, a possible cubic spacecraft may dock on any of its six sides, refer to Fig. 3. The dotted lines represent possible docking orientations. A spacecraft with only one male and female connection is very limited in versatility of assembly scenarios.

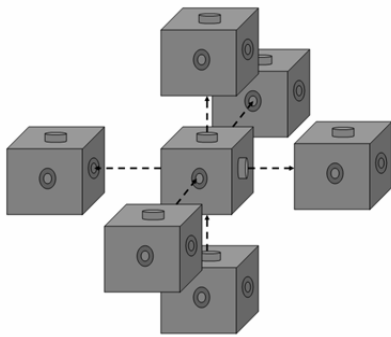


Figure 3: General Spacecraft Docking

The results for the six Chase spacecraft simultaneously docking with collision avoidance are listed in Table 9, with the far docking results listed in Table 10. For these collision avoidance maneuvers, the goal positions are docking ports on the surface of the Target

Table 9: Six Spacecraft Near Docking Maneuver

Near Docking	LQR/APF	APF
Near with Obstacle RSW [0, 70, 0]	$\Delta v = 0.3355$ $t_d = 1135$	$\Delta v = 0.2960$ $t_d = 1282$
Near with Obstacle RSW [50, -100, -50]	$\Delta v = 0.5694$ $t_d = 1118$	$\Delta v = 0.5648$ * $t_d = 1304$
Near with Obstacle RSW [100, 100, 100]	$\Delta v = 0.9915$ $t_d = 1355$	$\Delta v = 1.1742$ * $t_d = 1516$
Near with Obstacle RSW [100, 0, 0]	$\Delta v = 0.6902$ $t_d = 1307$	$\Delta v = 0.7264$ * $t_d = 1444$
Near with Obstacle RSW [-50, 100, -100]	$\Delta v = 0.9969$ $t_d = 1521$	$\Delta v = 0.7238$ * $t_d = 1397$
Near with Obstacle RSW [0, 0, 100]	$\Delta v = 0.7399$ $t_d = 1794$	$\Delta v = 0.6945$ * $t_d = 1923$

Table 10: Six Spacecraft Far Docking Maneuver

Far Docking	LQR/APF	APF
Far with Obstacle RSW [0, 1000, 0]	$\Delta v = 4.1792$ $t_d = 1530$	$\Delta v = 3.7513$ * $t_d = 1478$
Far with Obstacle RSW [412, -812, -412]	$\Delta v = 4.5243$ $t_d = 1870$	$\Delta v = 4.1084$ * $t_d = 1488$
Far with Obstacle RSW [575, 575, 575]	$\Delta v = 4.7083$ $t_d = 1719$	$\Delta v = 5.2832$ * $t_d = 1549$
Far with Obstacle RSW [1000, 0, 0]	$\Delta v = 4.9268$ * $t_d = 1520$	$\Delta v = 5.2024$ * $t_d = 1602$
Far with Obstacle RSW [0, 0, 1000]	$\Delta v = 3.6151$ $t_d = 1678$	$\Delta v = 3.8136$ * $t_d = 1496$
Far with Obstacle RSW [707, 707, 0]	$\Delta v = 3.0789$ $t_d = 1463$	$\Delta v = 5.1804$ * $t_d = 1509$

spacecraft. The maneuver is completed when the assigned spacecraft approaches within 2.0 mm of the center of the docking port. For the maneuvers shown, the docking ports are centered on each side of a cubic Target spacecraft at RSW locations of [1, 0, 0], [0, -1, 0], [0, 1, 0], [-1, 0, 0], [0, 1, 0], and [0, -1, 0], respectively. The 2.0 mm docking precision was selected, due to expected limits in sensor accuracy. Stationary obstacles are still placed the Chase spacecraft's path. In each case, collision avoidance of the stationary obstacles and other spacecraft was successful. The APF algorithm forces a strict return to the desired velocity once an obstacle is avoided. So, the APF tends to pull the spacecraft around obstacles faster than the LQR/APF, but risks saturating available actuation. The LQR/APF maneuver durations tend to be slightly longer due to smoother transitions in and out of obstacle regions.

Comparison of the control requested and the saturation limits for both algorithms, illustrates the smooth performance of the LQR/APF algorithm. The relative

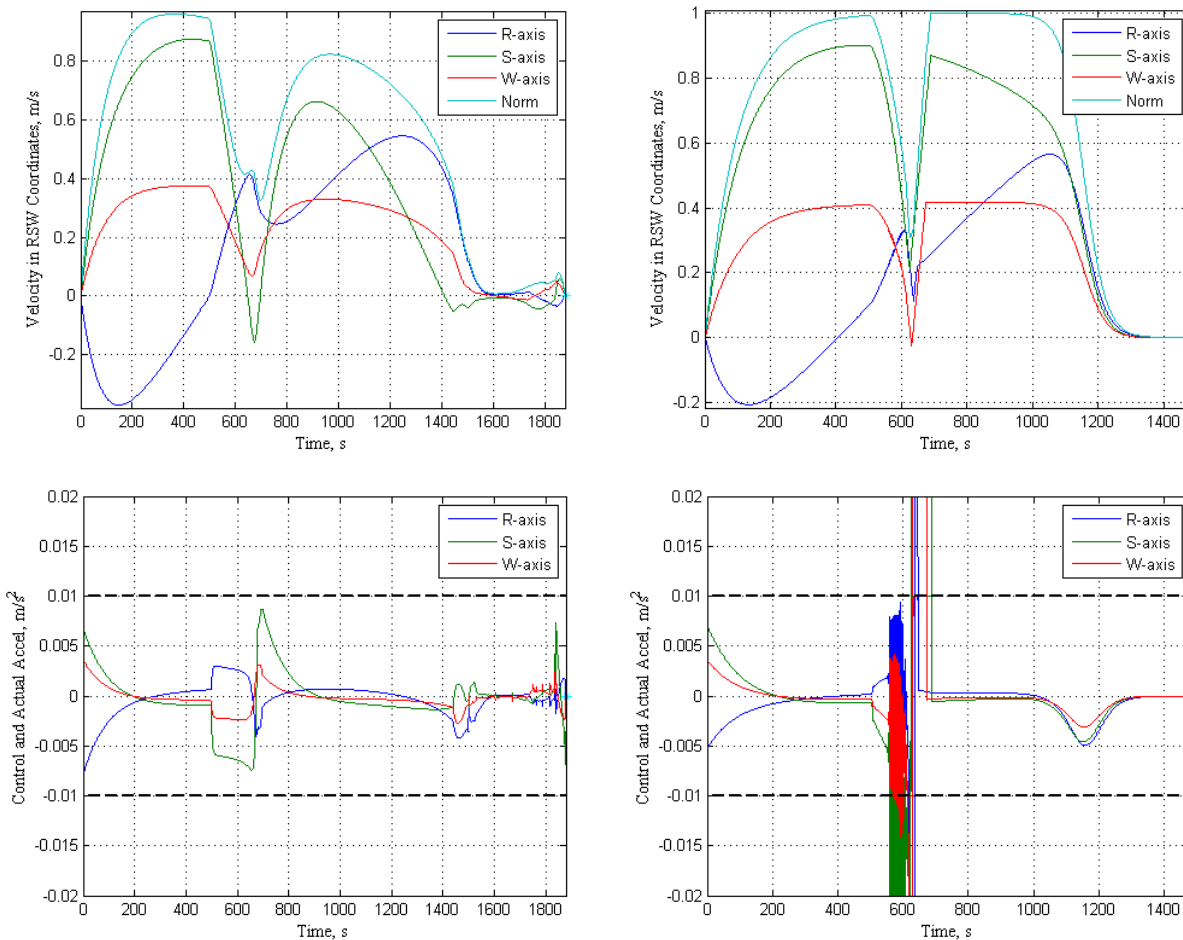


Figure 4: Performance Comparison of LQR/APF (left) and APF (right) during Docking Maneuver

velocity and acceleration of the Chase spacecraft's docking maneuver for the 2nd row of Table 10 is shown in Fig. 4. The central spike in velocity and acceleration, at approximately 600 s, is due to the stationary obstacle along the path. The last acceleration response is due to collision avoidance of the Target and other docking spacecraft. The dashed line on the acceleration plots show the thruster saturation limits. The desirable performance of the LQR/APF with collision avoidance is evident due to the excellent control effort response.

CONCLUSION

An autonomous distributed LQR/APF control algorithm for multiple small spacecraft in close proximity operations is proposed. The control algorithm combines LQR efficiency with APF based collision avoidance. The multiple spacecraft simulation results are promising. Future work may include research into the control algorithm robustness with random initial configurations and measurement uncertainty. The control algorithm may be further evaluated in a

hardware-in-the-loop laboratory test-bed. Development of the NPS Autonomous Multi-Agent Physically Interactive Spacecraft (AMPHIS) is being conducted concurrently with this research and should allow for future testing and validation of multiple spacecraft control concepts.³⁶⁻³⁷

ACKNOWLEDGMENTS

S. B. McCamish gratefully acknowledges the support from both faculty and students at the Naval Postgraduate School (NPS). The NPS Spacecraft Servicing and Robotics Laboratory is funded in part by the Defense Advanced Research Projects Agency (DARPA).

REFERENCES

1. Mathieu, C. and A.L Weigel, "Assessing the Flexibility provided by Fractionated Spacecraft," Proceedings of Space 2005 Conference, American Institute of Aeronautics and Astronautics (AIAA) 2005-6700, Long Beach, CA, Aug. 2005.

2. Brown, O., P. Ermenko., and C. Roberts, "Cost Benefit Analysis of a Notational Fractionated SATCOM Architecture," 24th International Communications Satellite Systems Conference (ICSSC), AIAA 2006-5328, San Diego, CA, June 2006.
3. Chen, Y.Q., and Z. Wang, "Formation Control: a Review and a New Consideration," Proceedings of IEEE/RSJ International Conference on Intelligent Robots and Systems (IROS), Edmonton, Alberta, Canada, Aug. 2005, pp. 3181 – 3186.
4. Ren, W., and R.W Beard, "Formation Feedback Control for Multiple Spacecraft via Virtual Structure," IEEE Proceedings of Control Theory and Applications, Vol. 151, No. 3, 23 May 2004, pp. 357-368.
5. Air Force Research Laboratory (AFRL), "XSS-11 Fact Sheet," URL: <http://www.vs.af.mil/FactSheets/XSS11-MicroSatellite.pdf> [cited 22 Jan. 2007].
6. Defense Advanced Research Projects Agency (DARPA), "Orbital Express Space Operations Architecture," URL: <http://www.darpa.mil/tto/programs/oe.htm> [cited 22 Jan. 2007].
7. David, L., "Military Micro-Sat Explores Space Inspection, Servicing Technologies," Technology [online periodical], 22 July 2005 URL: http://www.space.com/business/technology/050722_XSS-11_test.html [cited 20 July 2006].
8. Davis, T.M., T.L. Baker, T.T. Belchak and W.R. Larsen, "XSS-10 Micro-Satellite Flight Demonstration Program," Proceedings of the 17th Annual AIAA/USU Conference on Small Satellites, Logan, UT, Aug. 2003.
9. Dornheim, M.A., "Orbital Express to Test Full Autonomy for On-Orbit Service," Aviation Week & Space Technology (AW&ST), 4 June 2006 URL: http://www.aviationnow.com/avnow/news/channel_awst_story.jsp?id=news/aw060506p1.xml [cited 22 Sep. 2006].
10. Neubauer, J.S., "Controlling Swarms of Micro-Utility Spacecraft," DSc Thesis, Department of Mechanical and Aerospace Engineering, Washington University, Saint Louis, MO, 2006.
11. Neubauer, J.S. and M.A. Swartwout, "Controlling Swarms of Bandit Inspector Spacecraft," Proceedings of the 20th Annual AIAA/USU Conference on Small Satellites, Logan, UT, August 2006.
12. Mendy, P., "Multiple Satellite Trajectory Optimization," Masters Thesis, Mechanical and Astronautical Engineering Dept., Naval Postgraduate School, Monterey, CA, 2004.
13. McCamish, S.B., M. Romano, and X. Yun, "Autonomous Distributed Control Algorithm for Multiple Spacecraft in Close Proximity Operations," AIAA Guidance, Navigation and Control Conference, Hilton Head, SC, August 2007 (submitted for publication).
14. Vallado, D.A., *Fundamentals of Astrodynamics and Applications*, 2nd ed., Microcosm Press, El Segundo, CA, 2001.
15. Clohessy, W.H. and R.S. Wiltshire, "Terminal Guidance System for Satellite Rendezvous," Journal of the Aerospace Sciences, Vol. 27, No. 9, 1960, pp. 653-658.
16. Matlab and Simulink, The MathWorks Incorporated, URL: <http://www.mathworks.com/> [cited 18 September 2006].
17. Satellite Tool Kit (STK), Analytical Graphics Incorporated (AGI), URL: <https://www.agi.com/products/desktopApp/stkFamily> [cited 10 September 2006].
18. McCamish, S.B. and M. Romano, "Simulations of Relative Multiple-Spacecraft Dynamics and Control by MATLAB-Simulink and Satellite Tool Kit", AIAA 2007 Modeling and Simulation Technology Conference, Hilton Head, SC, August 2007 (submitted for publication).
19. Larson, W.J. and J.R. Wertz, *Space Mission Analysis and Design*, 3rd ed., Microcosm Press, El Segundo, CA, 2004.
20. Sidi, M.J. *Spacecraft Dynamics and Control*, Cambridge University Press, New York, NY, 1997.
21. Wie, B., *Space Vehicle Dynamics and Control*, AIAA, Reston, Virginia, 1998.
22. Khatib, O., "Real-Time Obstacle Avoidance For Manipulators and Mobile Robots," Proceedings of the International Conference on Robotics and Automation, Vol. 2, Mar. 1985, pp.500-505.
23. Koditschek, D.E., "Exact Robot Navigation by Means of Potential Functions: Some Topological Considerations," Proceedings of the International Conference on Advanced Robotics (ICAR), Vol. 4, March 1987, pp. 1-6.
24. Newman, W.S. and N. Hogan, "High Speed Robot Control and Obstacle Avoidance using Dynamic Potential Functions," Proceedings of

- the IEEE International Conference on Robotics and Automation, Vol. 4, March 1987, pp. 14-24.
25. Rimon, E. and D.E. Koditschek, "Exact Robot Navigation Using Artificial Potential Functions," IEEE Transactions on Robotics and Automation, Vol. 8, No. 5, October 1992, pp. 501-518.
 26. Guldner, J. and V.I. Utkin, "Sliding Mode Control for Gradient Tracking and Robot Navigation Using Artificial Potential Fields," IEEE Transactions on Robotics and Automation, Vol. 11, No. 2, April 1995, pp. 247-254.
 27. Yun, X. and K. Tan, "A Wall-Following Method for Escaping Local Minima in Potential Field Based Motion Planning," Proceedings of the International Conference on Advanced Robotics (ICAR), July 1997, pp. 421-426.
 28. Gazi, V., "Swarm Aggregation Using Artificial Potentials and Sliding Mode Control," IEEE Transactions on Robotics and Automation, Vol. 21, No. 6, Dec. 2005, pp. 1208-1214.
 29. McInnes, C.R., "Autonomous Proximity Maneuvering Using Artificial Potential Functions," European Space Agency Journal, Vol. 17, No. 2, 1993, pp. 159-169.
 30. McInnes, C.R., "Distributed Control of Manouvring Vehicles for On-Orbit Assembly," Journal of Guidance Control and Dynamics, Vol. 18, No. 5, Sep.-Oct. 1995, pp. 1204-1206.
 31. Lopez, I. and C.R. McInnes, "Autonomous Rendezvous Using Artificial Potential Function Guidance," Journal of Guidance Control and Dynamics, Vol. 18, No. 2, March-April 1995, pp. 237-241.
 32. McQuade, F., "Autonomous Control for On-Orbit Assembly Using Artificial Potential Functions", PhD Thesis, Department of Aerospace Engineering, University of Glasgow, Scotland, UK, 1997.
 33. Umehara, H. and C.R. McInnes, "Penalty-Function Guidance for Multiple-Satellite Cluster Formation," Journal of Guidance Control and Dynamics, Vol. 28, No. 1, Jan. 2005, pp. 182-185.
 34. Khalil, H.K., *Nonlinear Systems*, 3rd ed., Prentice Hall, Upper Saddle River, NJ, 2002.
 35. Yang, G., Q. Yang, V. Kapila, D. Palmer and R. Vaidyanathan, "Fuel Optimal Manoeuvres for Multiple Spacecraft Formation Reconfiguration Using Multi-Agent Optimization," *International Journal of Robust and Nonlinear Control*, Vol. 12, Feb.-March 2002, pp. 243-283.
 36. Romano, M. and J. Hall, "A Test Bed for Proximity Navigation and Control for Spacecraft for On-orbit Assembly and Reconfiguration," IEEE 2007 Advanced Intelligent Mechatronics Conference (submitted for publication).
 37. Romano, M., D.A. Friedman, and T.J.Shay, "Laboratory Experimentation of Autonomous Spacecraft Approach and Docking to a Collaborative Target," AIAA Journal of Spacecraft and Rockets, Vol. 43, No.1, Jan.-Feb. 2007.